

IISc THESES ABSTRACTS

Thesis Abstract (Ph.D.)

Investigation on the sex-specific organisation of chromatin and its relationship to genomic imprinting in the mealybug *Planococcus lilacinus* by Sanjeev Khosla

Research supervisor: Dr Vani Brahmachari

Department: Molecular Reproduction, Development and Genetics

1. Introduction

The term genomic imprinting defines a process that reversibly marks one of the two homologous loci, chromosomes or chromosomal sets during development, resulting in functional non-equivalence of genes. It involves not only a mechanism to mark the concerned genes or chromosomal regions depending on their parental origin but also mechanisms which can recognize, maintain and then erase the marking to allow the system to remark on the basis of sex of the progeny.¹ Genomic imprinting is known to occur in some insects and higher eukaryotes and is particularly well studied in mammals. In mammals, zygote with both the genome complements from the same parent does not develop to term suggesting the non-equivalence of genetic information inherited from the two parents.² Studies on coccids, a group of insects belonging to the order hemiptera, and sciara, a dipteran, also point to similar non-equivalence of parental genomes.¹

Mealybugs with 50% of their genomes subjected to these effects provide an excellent system to dissect out the mechanisms involved in imprinting. No sex chromosomes are reported in mealybugs and all the zygotes have the same chromosomal constitution. During embryogenesis, heterochromatization of an entire set of chromosomes takes place in some embryos during the cleavage stage. These embryos develop into males and the others into females. It has been shown that the set of chromosomes that get heterochromatized in males is of paternal origin.¹ Thus, in mealybugs, heterochromatization or chromatin organisation is not only related to sex determination but also to phenomenon of genomic imprinting. To investigate the relationship of heterochromatization with genomic imprinting, the understanding of chromatin organisation in this insect is essential. Furthermore, it would be necessary to know peculiarities, if any, in the chromatin organisation in male mealybugs.

2. Results and discussion

In a comparative study of chromatin from male and female mealybugs of the species, *Planococcus lilacinus*, it was found that a fraction of chromatin in male mealybugs is resistant to digestion by micrococcal nuclease.^{3, 4} This fraction of chromatin designated as nuclease-resistant chromatin (NRC) is observed only in male mealybugs in which the paternal complement of the genome is heterochromatized, thus suggesting a relation between NRC and

the condensed state of paternal chromosomes in the males. NRC fraction constitutes only 8–10% of the male genome as against cytologically visible heterochromatization which constitutes 50% of the male genome. Thus, it probably has a functional significance in heterochromatization.

Analysis of NRC showed that DNA sequences representing NRC are not specific to males but found in both the sexes. Even in females, they are organised into a chromatin fraction which is more nuclease resistant as compared to the rest of the genome. Seventy per cent of the tissue in adult male mealybugs is sperm bundle and it is known that chromatin in sperms is organised in a highly compact manner different from that in somatic nuclei. However, it was found that in male mealybugs this chromatin fraction is present in both somatic and sperm nuclei, negating the possibility of NRC being a sperm contribution. The association of histones with NRC confirmed that the primary organisation of NRC into chromatin was nucleosomal. Therefore, the unusual organisation of NRC is probably manifested at the level of higher-order chromatin structure.

An examination of the DNA representing NRC revealed that it is heterogeneous with respect to size and sequence. Large DNA sequences in the range of 2–100 kb are organised into NRC. Southern hybridisation of NRC DNA with mealybug genomic DNA also suggests that certain sequences within NRC DNA are present in multiple copies. To investigate the nature of NRC DNA, an analysis of the NRC DNA was undertaken by cloning *Sau3AI* fragments of NRC DNA into the *Bam* HI site of the Bluescript vector pSK (II)+. The NRC-specific clones that have been designed as *nrc* (#) were found to be unstable in *E. coli* cells. Sequences have an A+T content in the range of 58–71%. None of the NRC sequences have any appreciable similarity to known DNA sequences available in the DNA data bank (GenBank). We have not been able to detect any open reading frame (ORF) of appreciable length in any of the clones. Certain motifs are observed within some of the NRC sequences. An adenine-rich motif, known to be present in the alpha satellite sequence of the mouse-centromeric DNA, is present in *nrc7* and *nrc8*. Matrix- or scaffold-associated region (MAR or SAR) motifs which are involved in the attachment of DNA to the nuclear matrix are present in several of the NRC clones. Some of the sequences contain very long stretches of adenine and thymines. Within *nrc50* sequence a pentanucleotide 'CACTA' is tandemly repeated five times as also a hexanucleotide "ACGTCC" which is tandemly repeated six times.

It was shown by Brown and Nelson-Rees,⁵ and Chandra⁶ that fragmented chromosomes inherited from father can heterochromatize in the sons. This property is shown even by the smallest of the chromosomal fragments inherited from the father.⁶ This would suggest that the centres which could initiate chromosomal condensation are present at several loci on each chromosome in contrast to the case of a single inactivation centre on the mammalian X chromosome. In the light of these results, the possibility of a subset of NRC DNA sequences performing a specialised role is examined, one such function being the capacity to act as nucleation centres for heterochromatization. In this context, some of the attributes expected of multiple nucleation centres in mealybugs would be: (1) The DNA sequences must occur in multiple copies and be dispersed throughout the genome. (2) If a subset of NRC sequences is to be centre of activation, then most fragments within NRC must include at least one such sequence

to facilitate the observed organisation. (3) Given all the factors necessary for NRC organisation, such putative centres should be capable of inducing inactivation *in vitro*.

We have tested the plasmid clones derived from NRC DNA for a validity of attributes 1 and 2. Our preliminary results suggest that at least two NRC DNA clones, *nrc50* and *nrc51*, fulfill the criteria mentioned in attributes 1 and 2.

Analysis of the factors that contribute to nuclease-resistant organisation of a fraction of chromatin in male mealybugs revealed two more properties of this fraction of chromatin in male mealybugs. In addition to nuclease resistance, it was found that DNA sequences in this fraction were compactly organised into chromatin and were associated with nuclear matrix. Association of chromatin with the matrix has been suggested as a means of higher-order chromatin organisation in other systems where 300–5000-bp-long DNA sequences anchor large loops of chromatin to the nuclear matrix or nuclear scaffold. Such anchoring DNA sequences are termed MARs or SARs. DNA fragments within NRC which range in size from 2 to 100 kb thus represent unusually long DNA sequences associated with nuclear matrix. It is interesting to note that several clones derived from NRC DNA contain the A + T-rich motif implicated in nuclear matrix association. This observation is significant as an aspect of the unusual organisation of NRC.

The relationship between nuclease resistance, compaction and matrix association of NRC was investigated. The results suggest that the association of NRC with nuclear matrix confers nuclease resistance. NRC can be dissociated from nuclear matrix while retaining compaction; similarly, compactness can be lost while being matrix associated. However, it is possible that *in vivo*, compaction and nuclear matrix association are acting together or organise NRC into a nuclease-resistant organisation.

Southwestern analysis to identify proteins that interact with NRC to confer it the nuclease resistance suggests that a 30–35 kDa protein binds with NRC DNA. It was found that *Drosophila* DNA, used as non-specific in binding assays, binds very strongly to the 30–35 kDa protein present in the soluble fraction of the nuclei of male mealybugs but its binding is very weak to a similar molecular weight protein present in the matrix fraction of chromatin derived from male mealybugs. The observations made so far probably suggest the presence of proteins of similar molecular weight in the two sexes, which differ in their localisation within the nuclei. Preliminary results suggest the presence of this 30–35 kDa protein in the matrix fraction of only young male mealybugs and crawlers.

The three properties of NRC, namely, nuclear resistance, compaction and matrix association elucidated in the study are easily assayable properties that can be used to understand the functional significance of DNA sequences organised as NRC.

References

1. BROWN, S. W. AND CHANDRA, H. S. *Cell biology: A comprehensive treatise*, Vol. 1. Academic Press, 1977, pp. 109–189.
2. OHLSSON, R., HALL, K. AND RITZEN, M. (EDS) *Genomic imprinting: Causes and consequences*. Cambridge University Press, 1995.

3. KANTHETI, P. *Studies on a female-specific cDNA clone, and chromatin organization, in a mealybug, Planococcus lilacinus*, Ph.D. Thesis, Institute of Science, Bangalore, 1997.
4. KHOSLA, S. *et al.* *Chromsoma*, 1996, **104**, 386–392.
5. BROWN, S. W. AND NELSON-REES, W. A. *Genetics*, 1961, **46**, 983–1007.
6. CHANDRA, H. S. *Chromosoma*, 1963, **14**, 230–246.

Thesis Abstract (Ph.D.)

Insertion reactions of copper(I) aryloxides with heterocumulenes by Christina Baskaran (née Wycliff)

Research supervisor: Prof. A. G. Samuelson

Department: Inorganic and Physical Chemistry

1. Introduction

Studies on alkoxide and aryloxide complexes of copper (I), a late transition metal ion, are important as the mismatch of the 'soft' metal center and the 'hard' oxygen donor leads to enhanced reactivity.¹ Apart from the biological significance of the Cu(I)–OR bond, copper(I) alkoxides have gained importance in small molecule activation. Detailed investigations on the reactions of small molecules like CO₂ and CS₂ with CU(I) are sparse although reactions of these heterocumulenes with other transition metals such as molybdenum, tungsten and iridium have been reported recently.²

In the present investigation, the insertion reaction of copper(I) aryloxide complexes with heterocumulenes (electronic analogs of CO₂ like CS₂ and RNCS, primarily MeNCS) has been studied. This reaction results in the *in-situ* formation of a substituted methanethiolate ligand complexed to copper. Oligomeric complexes having copper(I) ion bonded to soft donor ligands like sulfur and nitrogen are formed and are quite stable. The steric and electronic factors that govern the insertion reaction have been studied. The following equation shows the insertion of a heterocumulene across the CU(I)–OAr bond. The insertion is followed by a rearrangement and oligomerization.

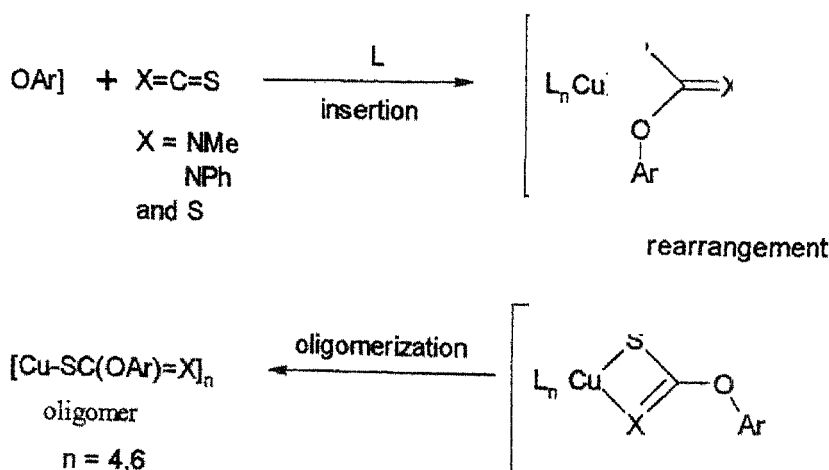

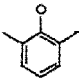
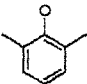
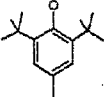
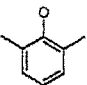


Table I

ARYLOXIDE	HETEROCUMULENE	PRODUCT
	Ph-N=C=S	HEXAMER
	Ph-N=C=S	HEXAMER
	Ph-N=C=S	HEXAMER
	Ph-N=C=S	TETRAMER
	Me-N=C=S	HEXAMER
	Me-N=C=S	HEXAMER
	Me-N=C=S	TETRAMER
	S=C=S	TETRAMER
	S=C=S	HEXAMER
	S=C=S	MULTIPLE INSERTIONS

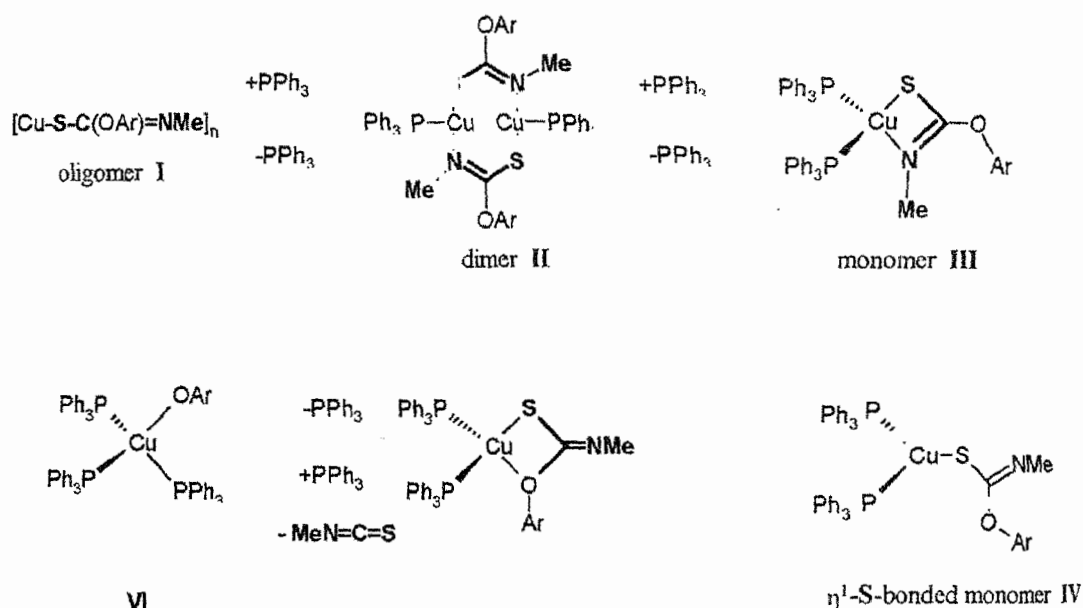
2. Role steric factors

Steric effects were found to dictate the structure and nuclearity of the resulting oligomeric complexes. Earlier studies with PhNCS have shown that the presence of sterically demanding substituents on the aryloxide led to the formation of species of lower nuclearity.³ In the present work, it has been shown that this steric congestion could be relieved by employing less bulky groups on the heterocumulene, thereby resulting in complexes of higher nuclearity even with bulky phenols. It has also been shown how a gradual reduction in the size leads to

more symmetry in structure of the resulting oligomeric complex. Thus, by introducing suitable steric variations in phenol and the heterocumulene, the structure and nuclearity of the oligomeric complexes could be controlled. Table I shows the reactants and nuclearity of the products.

3. Role of electronic factors

Electronic effects were also found to play an important role in the insertion reaction. While steric factors alter the structure of the product, electronic effects modify the reactivity patterns. The insertion reaction was found to be favorable when the carbon atom of the heterocumulene across the Cu(I)-OAr bond becomes reversible, which corresponds to unfavourable electronic factors. Electronic variations were introduced by employing heterocumulenes and aryloxides with varying electronic features. The insertion reaction of MeNCS, a less electrophilic heterocumulene, is reversible in the presence of PPh₃. Based on the reactivity patterns, a possible mechanistic pathway is postulated which is shown in the following equation.

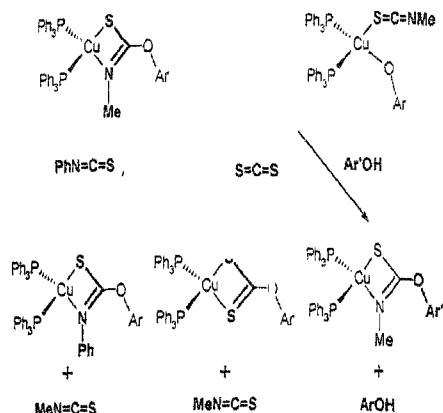


Similarly, the reactions with phenols having electron-withdrawing groups were also unfavorable.

4. Exchange reactions

The reversible nature of the insertion allows exchange of either the heterocumulene or the aryloxy group in the oligomeric complex in the presence of catalytic amounts of PPh₃. A less electrophilic heterocumulene could be substituted by a more electrophilic one and an electron-deficient aryloxy could be replaced by a more nucleophilic one.

The reversible behavior is apparently contrary to HSAB principles since a Cu-S bond is replaced with a Cu-O and shows the limitations of HSAB theory.

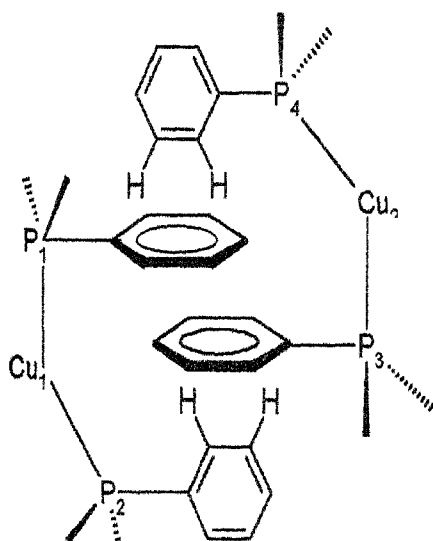


4.1. Bis-triphenylphosphine complexes of copper(I) with thione ligands

Treatment of these oligomeric complexes with PPh_3 results in the formation of bis-triphenylphosphine Cu(I)L species. The structures of these complexes were compared with those of copper(I) phosphine complexes of heterocyclic thiones as these two ligands are similar in structure. The comparison showed that the electronic properties of these ligands are different and as a result their bonding patterns are also different.

4.2. Supramolecular interactions in bis-triphenylphosphine complexes of copper(I)

Examination of the solid-state structures of these complexes revealed an interesting supramolecular motif. The phenyl rings of PPh_3 are involved in a concerted supramolecular interaction and this has been called the C-H π step.



The C-H π step is made up of a series of alternating C-H $\cdots\pi$ and $\pi\cdots\pi$ interactions among four phosphines attached to two different metal atoms.

References

- 1(a). BRYNDZA, H. E. AND TAM, W. *Chem Rev.*, 1988, **88**, 1163 and references therein.
- (b). KRAFFT, T. E., HEJNA, C. I. AND SMITH, J. S. *Inorg. Chem.*, 1990, **29**, 2682.
- (c). GLUECK, D. S., WINSLOW, L. J. N. AND BERGMAN, R. G. *Organometallics*, 1991, **10**, 1462.
- 2(a). GLUECK, D. S., WINSLOW, L. J. N. AND BERGMAN, R. G. *Organometallics*, 1991, **10**, 1462.
- (b). GIBSON, V. C., *et al.* *J. Chem. Soc., Chem. Commun.*, 1994, 2635.
- (c). DARENSBOURG, D. J. *et al.* *Inorg. Chem.*, 1991, **30**, 2418.
- 3(a). ABRAHAM, S. P. *et al.* *Inorg. Chem.*, 1993, **32**, 1739.
- (b). NARASIMHAMURTHY, N., SAMUELSON, A. G. AND MANOHAR, H. *J. Chem. Soc., Chem. Commun.*, 1989, 1803.

Thesis Abstract (Ph. D.)

Time-resolved resonance Raman spectroscopic studies on photoinduced transients by R. Anandhi

Research supervisor: Dr. S. Umapathy

Department: Inorganic and Physical Chemistry

1. Introduction

A study of reactive intermediates is of primary importance to understand the mechanistic aspects of photochemical reactions. Various spectroscopic methods have been employed to probe the structure and dynamics of short-lived intermediates. Flash photolysis and pulse radiolysis techniques are commonly used to obtain the absorption spectra of the excited states and radicals which are short-lived. However, the absorption spectra of intermediates with similar spectral features lead to ambiguity in understanding the photochemistry of kinetically different but structurally similar intermediates. In contrast, time-resolved vibrational spectroscopic methods are superior to absorption techniques to elucidate the structure of the intermediates in detail. Therefore, in the present study, time-resolved resonance Raman spectroscopy has been utilized to study the structure of short-lived intermediates of decafluorobenzophenone and carbazole derivatives.

2. Experimental methods

An experimental set-up has been developed for the time-resolved resonance Raman spectroscopic studies, a part of which includes the fabrication of a Raman shifter to tune the laser wavelength. The performance of the Raman shifter has been evaluated using methane and hydrogen gases. The experimental set-up has been standardized by comparison with the reported time-resolved resonance Raman of benzophenone.

3. Results and discussion

3.1. Carbazole system

Polyvinylcarbazole is a well-known photoconducting polymer.¹ In a photoconducting polymer, photogeneration of carriers followed by transport of carriers are important steps during photoconduction. In polyvinylcarbazole and other photoconducting polymers with carbazole chromophore, photoconduction has been reported to take place by hole (radical cation).² Time-resolved absorption and fluorescence studies have been utilized to understand the mechanistic aspects of the charge carrier generation in polyvinylcarbazole. Though the transient absorption and time-resolved fluorescence studies give information about kinetic and mechanistic aspects of photoinduced charge carrier formation in polyvinylcarbazole, they do not provide any information on the structure of the charge carrier. The structure of the radical cation of polyvinylcarbazole in comparison with its model compound, N-ethylcarbazole, in terms of delocalization of the odd electron in the polymer chain, is expected to provide structural clues regarding electrical and photoconduction mechanism. Therefore, the present investigation involves the study of the structure of the charge carriers in photo- and electrically conducting polyvinylcarbazole. During the present study, the Raman spectra of the neutral carbazoles and the resonance Raman spectra of various cations, such as mono-, di- and polymer radical cations have been assigned. Further, the structure of these radical cations have been inferred by comparing our experimental results with theoretical results. The evidence for partial exchange of the odd-electron in dimer radical cation in the polymer chain with neutral species has been found by our Raman studies.

A part of the work in this system also involves transient absorption studies of polyvinylcarbazole and its dibromoderivative. The mobility and the efficiency of charge carrier formation together can affect photoconductivity. Earlier reports on NMR spectroscopy revealed that the mobility of charge carrier in polyvinylcarbazole is related to the structure of the polymer. In the present work, it has been observed that the charge carrier (radical cation) formation efficiency also depends on the structure of the polymer. The yield of the radical cation in the dibromopolyvinylcarbazole has been found to be an order of magnitude less than that of polyvinylcarbazole. In polyvinylcarbazole, the ratio of monomer to polymer radical cation yield is 2.0. The difference in the yields has been attributed to the steric effect of the bulky bromine group in dibromopolyvinylcarbazole.

3.2. Decafluorobenzophenone system

Intermolecular hydrogen atom abstraction is ubiquitous in organic photochemistry.³ The efficiency and reactivity of the photoexcited states toward the abstraction process is reported to depend on the multiplicity and configuration of the electronic excited state, interactions between the hydrogen donor and the acceptor, and the influence of the solvent.³ These aspects have been studied widely by various experimental methods, including transient absorption spectroscopy.⁴

Benzophenone is a prototypical molecule which undergoes hydrogen atom abstraction from its lowest triplet excited state, and the photochemistry and photophysics are well understood.⁵ Transient absorption studies have been used to elucidate the mechanism of hydrogen

abstraction, both in benzophenone and decafluorobenzophenone. In fact, decafluorobenzophenone undergoes similar photophysics and photochemistry, but the triplet excited state is far more reactive than benzophenone. The lowest triplet excited state energy of benzophenone and decafluorobenzophenone is very similar, 69 kcal/mole, and the triplet quantum yield is equal to 1 for both. However, the reactivity of decafluorobenzophenone triplet state is orders of magnitude higher than that of benzophenone. Therefore, the objective of the present study is to demonstrate the utility of time-resolved resonance Raman method to study photoinitiated reactions and to understand the structure–reactivity correlations in benzophenone and decafluorobenzophenone systems.

From our present study, higher reactivity of perfluorinated derivative of benzophenone over benzophenone has been addressed by time-resolved resonance Raman investigation. The analyses of the results on triplet state and the ketyl radical of decafluorobenzophenone show that the unpaired electron of the triplet state is localized on the carbonyl group. The localization of the spin is due to spin-destabilizing nature of the fluorine. It is concluded that the higher reactivity of decafluorobenzophenone over benzophenone can be attributed to (a) non-planar structure of the triplet excited state of decafluorobenzophenone compared to benzophenone, thus increasing the accessibility to the carbonyl group and (b) highly polarized and electrophilic nature of the carbonyl group in the triplet excited state.

References

1. MYLNIKOV, V. S. *Advances in polymer science*, Vol. 115, 1994, pp. 1-
2. MORT, J. AND EMERALD, R. L. *J. Appl. Phys.*, 1974, **45**, 175–178.
3. WAGNER, P. AND PARK, B. S. *Organic Photochem.*, 1991, **11**, 227–366.
4. SHOUTE, C. T. L. AND MITTAL, J. P. *J. Phys. Chem.*, 1993, **97**, 8630–8637.
5. BARTHALOMEV, R. F. *et al.* *J. Chem. Soc., Perkin Trans.*, 1972, **2**, 577–582.

Thesis Abstract (M. Sc. (Engng))

Modelling and characterization of sprayformed 7075 aluminium alloy and a composite with Al₂O₃ by C. Sanjivi

Research supervisors: Profs S. Ranganathan and A. K. Lahiri

Department: Metallurgy

1. Introduction

Sprayforming¹ is an innovative processing technique in the present demanding world to satisfy the stringent conditions laid down by metallurgical quality considerations as well as economy. Atomization and deposition are two steps involved in this process, whereby disintegration of the molten alloy stream into fine micron-sized droplets by high-velocity gas and the collection of droplets on to the substrate takes place, respectively. The main advantage of this

processing method is that it involves semi-solid state processing conditions and can be classified in a regime between ingot and powder metallurgy. Fine equiaxed grains, devoid of macrosegregation, extension in solid solubility and novel alloy compositions are typical characteristics² of this synthesizing procedure. In the present study, synthesis and characterization of 7075 aluminium alloy and a composite with Al_2O_3 were carried out. This is followed by mathematical modelling³ to understand the process synergism to study the effect of process parameters on the microstructural evolution.

2. Spray atomization

The atomization stage^{4, 5} deals with dynamical, thermal and solidification effects experienced by alloy droplets during their flight to the deposit. All the droplets were considered to undergo the following thermal regimes, namely, cooling in liquid state, nucleation and recalescence, equilibrium solidification and finally cooling in solid state. Forced convective heat transfer by atomizing gas is the predominant mode of heat removal from the atomized droplets. The velocity profiles of atomizing gas and atomized droplets were studied along with variation in temperature, fraction solidified and cooling rate experienced by droplets of varying diameters. The observed microstructures in the oversprayed powders were investigated and it was found that the type of solidification encountered is different from conventional directional solidification. The theory proposed by Kurz and Fischer⁶ explains satisfactorily the equiaxed dendritic morphology (Fig. 1) observed in the oversprayed powders, where as the growth rate goes down, the morphology changes from spherical to cellular to dendritic. Cooling rate experienced by the atomized droplets was found to be of the order of 10^4 to 10^5 . The mass distribution of the oversprayed powders was found to be Gaussian in nature. An estimate of enthalpy of the spray reaching the deposit was predicted on the basis of temperature profile experienced by the droplets and droplet/powder distribution of oversprayed powders. The effect of process parameters such as velocity of the atomizing gas, the melt superheat, the flight distance and also the undercooling on the thermal and solidification profiles of the atomized droplets was studied. It was found that undercooling can be effective in affecting the microstructure of very fine droplets.

3. Spray deposition

The deposition stage is concerned with the prediction of grain size variations across the deposit. The microstructure across the deposit thickness is determined primarily by two competing parameters,⁷ namely, the deposition rate and the rate of solidification. One-dimensional heat-balance equation based on enthalpy formulation is used in predicting the thermal profiles, the cooling rates and the iso-solid fraction lines in the deposit. Conductive heat transfer by the substrate and convective heat transfer by the atomizing gas were considered as major modes of heat dissipation from the deposit. Implicit mode of solving partial differential equations with simple initial temperature profile across the deposit was adopted and found to be computationally efficient and stable. Shape and temperature profile across the deposit was adopted and found to be computationally efficient and stable. Shape and temperature profiles of the deposit during and after deposition were carried out to understand the temperature and solidification conditions. The isolated effects of changes in value of the process parameters

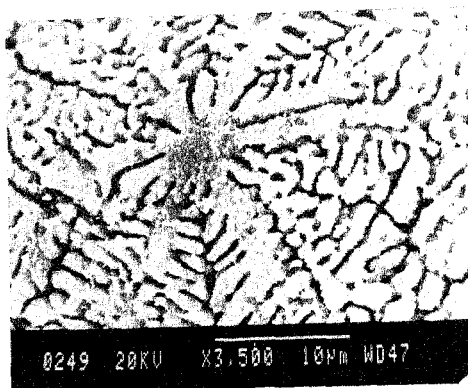


FIG. 1. Equiaxed dendritic solidification inside an atomized powder.

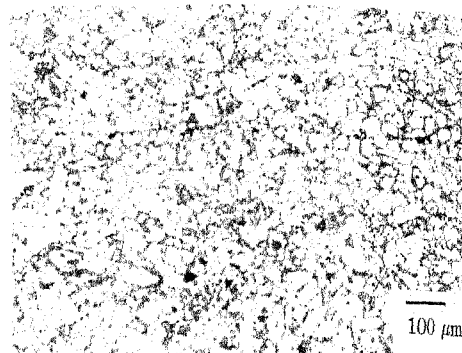


FIG. 2. Equiaxed grain structure of spray-formed 7075 aluminium alloy.

starting with changes in the melt flow rate, the heat-transfer coefficient at the deposit substrate interface as well as at droplet gas interface.

The overall microstructure of the spray deposit was found to be fine equiaxed grain in nature. Grain size (Fig. 2) was found to vary from 15 to 45 μm . Presolidified droplets as well as dendrites in the partially solidified droplets serve as nuclei for the solidification at the deposit. An increase in the nucleation sites can be viable as fragmenting and fracturing of the dendrites. Fine equiaxed nature⁸ of the grains in spite of low cooling rate at the deposit (1-50 K/s) can be attributed to constrained grain growth due to increased nucleation sites. About 20 to 30% of liquid content in the semi-solid slush is important to stay froth at the surface of the deposit during processing to have a desirable microstructure, namely, fine-grain microstructure with a low amount of porosity. Layered microstructures prevailing in the deposit indicate that the splatting process is quicker than the solidification mechanism. Pores in the deposit can be attributed to entrapment of the atomizing gas and also due to insufficient metal flow to fill the interstices formed between droplets falling at the deposit.

4. Spray co-deposition

Spray co-deposition⁹ involves an additional step of injecting Al_2O_3 particulates into the molten alloy stream. The effect of ceramic particulates on thermal and solidification behaviour of the alloy droplets during flight has been taken into consideration. Moreover, the role of ceramic particulates in thermal equilibration at the deposit is also significant. Modelling here is similar to that of spray deposition except that an additional mode of heat extraction by conductive heat transfer effected by ceramic particulates in contact with the droplets was considered in calculations. About 20% of thermal energy is carried away by Al_2O_3 particulates from the atomized droplets in the flight and about 10% from the deposit in the process of thermal equilibration.

The equiaxed structure observed in the base matrix is attributed to the high nucleation density at the deposit, constrained growth as well as to growth and coalescence of dendrites in the deposit. The spatially independent distribution of the Al_2O_3 particulates can be attributed

to entrapment by the presence of dendrite fragments which obstruct the motion of former in the semi-solid state prevailing at the deposit. The mechanical entrapment¹⁰ of the ceramic particulates by the droplets also proves to be a possible mechanism for the homogeneous distribution of ceramic particulates in the matrix.

References

1. SINGER, A. R. E. *Metall. Mater.*, 1970, 4, 246-250.
2. ANNAVARAPU, S., APELIAN, D. AND LAWLEY, A. *Metall. Trans. A*, 1988, 19, 3077-3094.
3. RAPPAZ, M. *Int. Mater. Rev.*, 1989, 34, 93-123.
4. GRANT, P. S., CANTOR, B. AND KATGERMANN, L. *Acta Metall. Mater.*, 1993, 41, 3097-3108.
5. LIANG, X., EARTHMAN, J. C. AND LAVERNIA, E. J. *Acta Metall. Mater.*, 1992, 40, 3003-3016.
6. KURZ, W. AND FISCHER, D. J. *Int. Metall. Rev.*, 1979, 5, 177-220.
7. MATHUR, P., APELIAN, D. AND LAWLEY, A. *Acta Metall.*, 1989, 37, 429-443.
8. LAVERNIA, E. J. *Int. J. Rapid Solidification*, 1989, 5, 47-98.
9. GUPTA, M., MOHAMED, F. A. AND LAVERNIA, E. *Metall. Trans. A*, 1992, 23, 831-843.
10. WU, Y. AND LAVERNIA, E. J. *Metall. Trans. A*, 1992, 23, 2923-2947.

Thesis Abstract

Thesis Abstract (Ph. D.)

Spectroscopic studies on the conformation and interaction of a channel forming cyclohexapeptide and a few selected neuropeptides by Jagannathan Ramesh

Department: Molecular Biophysics Unit

Research supervisor: Prof. K. R. K. Easwaran

1. Introduction

A knowledge of the structure and conformation of biomolecules such as peptides, proteins and nuclei acids is vital for the understanding of their function.¹ The techniques used for analysis, both in solid and solution state, have today advanced to an unprecedented level that one can understand the mechanism of action of various biological processes at the molecular level.²⁻⁴ Such studies have led to the design of biomolecules of desired function. This work is concerned with the structural elucidation and interaction studies on a few biologically important peptides such as cyclic hexapeptide cyclo(D-ala-L-pro-L-ala)₂ which possibly forms a channel inside the lipid bilayer by an assembly of several molecules and selected neuropeptides such as N-acetyl-L-aspartyl-L-glutamate (NAAG) and arg-phe-amide class of peptides. Techniques employed in this study are circular dichroism and nuclear magnetic resonance (NMR).

2. Materials and methods

2.1. CD studies

The CD spectra were recorded using a JASCO 500 Å spectropolarimeter equipped with a 501N data processor. The instrument was calibrated with 10-d-(+)-camphor sulphonic acid. Spectra were averaged over 4–8 accumulations. Quartz cells of pathlengths 1 and 2 mm were used. Solvent baselines were subtracted from sample spectra.

2.2. NMR studies

Proton NMR spectra were recorded on Bruker AMX 400, 500 MHz and Varian 600 MHz instruments. The resonance of residual protons of the solvent was used as an internal reference. All the 2D spectra (DQF-COSY and ROESY) were recorded in phase-sensitive mode, using the TPPI method with 512 t_1 . Recycling times (acquisition plus relaxation data) were about 1.8 s. The base lines of ROESY spectra were processed with a third-order polynomial. Only small oscillations were produced in the spectra. Finally, the data sets were generally symmetrized, although original data were carefully examined to verify that no artifact was introduced by symmetrization.

2.3. DSC studies

DSC thermograms were recorded with a computer-controlled Microcal-MC2 high-sensitivity differential scanning calorimeter (Microcal) operating at heating scan rate 90°C/h. The data acquired were analyzed with DA2 software and Microcal Origin softwares.

2.4. BLM conductance studies

Planar lipid bilayers were painted across a 0.3-mm-diameter hole in a styrene copolymer cup with *n*-decane dispersion of soybean lecithin (2% w/v) with and without the cyclic peptide. The concentration of the peptide used was 1×10^{-6} M. The styrene copolymer cup (*cis*) rested in an outer chamber (*trans*) and the bilayer partition, separated aqueous solution of similar ionic composition (100 mM NaCl, 5 mM CaCl₂ in 10 mM HEPES pH 7.5). A low-noise operational amplifier (OPA 102B, Burr-Brown) with frequency compensation was used. Electrical connection to the experimental chambers was through Ag-AgCl wires. Connections to the outer chamber were taken to the ground, while the *cis* side was taken to the non-inverting input of the operational amplifier. Potential difference was *cis* with respect to *trans*. Measurements were carried out at room temperature (25°C). The voltage and current signals were plotted using a pen recorder (Bryans UK). Formation of a bilayer was judged from the transients in the current traces due to membrane capacitance following application of 2-mV pulses.

3. Results and discussion

The results were obtained on the solution conformation of the channel forming cyclo(D-ala-L-pro-L-ala)₂ using spectroscopic techniques, UV, CD and NMR. UV and CD data showed that

the cyclic peptide has tendency to aggregate at higher concentration. Detailed 1 and 2D NMR studies showed that the free cyclo(D-ala-L-pro-L-ala)₂ in acetonitrile exhibits a structure with type I β -turn having L-pro in the I + 1 and L-ala in I + 2 positions. Also, in this conformation, all the carbonyl groups are on one side of the molecule and on NHs on the other. The observed conformation of this cyclic hexapeptide is compared with the reported data on related cyclic peptides. Studies on the ion-binding properties of cyclo(D-ala-L-pro-L-ala)₂ showed that this peptide binds strongly with calcium ion. Detailed NMR analysis showed that the proposed conformation for the cyclic peptide-calcium complex could be a 1:2 peptide: calcium complex. Each calcium ion is coordinated to three carbonyl oxygens. The remaining coordination is likely from the perchlorate anion or the solvent molecule. In a 2:2 peptide: calcium complex, each calcium ion is coordinated to six carbonyls, three from each peptide molecule of a dimeric complex. The results on the interaction of cyclo(D-ala-L-pro-L-ala)₂ with model membranes, investigated using CD and DSC, are also presented. CD data showed that the peptide undergoes a drastic change in conformation or aggregates when incorporated in lipid bilayers. DSC results gave evidence for possible aggregation of the peptide molecule in lipid bilayer affecting its fluidity. Bilayer membrane conductance (BLM) studies on cyclo(D-ala-L-pro-L-ala)₂ incorporated in bilayer membranes give evidence of a channel-like behaviour of the aggregated peptide in membranes.

Conformational studies on the acidic neurotransmitter, NAAG, in methanol and water at different pH values showed that while in methanol the peptide could assume a slightly folded structure stabilized by intramolecular hydrogen bonds, in water it gave a pH-dependent conformation. The α -COOH and side-chain carboxyl groups get deprotonated at pH above their pK_a values and this stepwise deprotonation affects the intramolecular hydrogen bond involving these groups and thereby alter the conformation of the peptide. Proton and ²⁷Al NMR studies of NAAG-Al-maltolate complex showed that NAAG binds to Al³⁺. CD and NMR studies on the interaction of NAAG with three important polyamines, namely, putrescine, cadaverine and spermine in water and methanol showed very interesting structures for the complexes in methanol derived from extensive 1 and 2D NMR data.

Conformational studies on arg-phe-amide(RF-NH₂) class of peptides, namely, phe-pet-arg-phe-NH₂ (FMRF-NH₂), pGlu-asp-pro-phe-leu-arg-phe-NH₂ (pQDPFLRF-NH₂), and pro-asp-val-asp-his-val-phe-leu-arg-phe-NH₂ (PDVDHVFLRF-NH₂) using CD and NMR showed that FMRF-NH₂ peptide showed that the tetrapeptide exists in extended conformation and binds strongly to calcium ion in acetonitrile. Detailed CD, 1 and 2D NMR studies on the heptapeptide, pQDPFLRF-NH₂, in methanol indicated that the peptide assumes a folded conformation with a head group region involving the first five residues and a linear tail portion involving the last two residues. The proposed conformation of the head group has a 1 \rightarrow 5 intramolecular hydrogen bond and a γ -turn having a 1 \rightarrow 3 hydrogen bond containing the proline residue. NMR studies on the decamer, PDVDHVFLRF-NH₂, in TMP solvent suggested that this peptide adopts an α -turn conformation comprising the first five residues. A bend structure comprising the last three residues at the C-terminal was also observed.

Some of the results obtained on the interaction of Al³⁺ a) with Tau protein, a microtubule associated protein implicated in Alzheimer's disease and b) with β -amyloid peptide using CD and ²⁷Al NMR are reported in the thesis.

4. Conclusions

This work deals with the structure and interaction of a channel-forming cyclic hexapeptide and two kinds of neuropeptides. The cyclic peptide chosen for the study, cyclo(D-ala-L-pro-L-ala)₂ showed interesting aggregation and metal ion-binding properties. Preliminary BLM studies showed that it has tendency to form channel in the lipid bilayer. CD studies indicated that the peptide binds calcium ion with high affinity among the metal ions studied. Detailed NMR studies revealed that the free peptide in acetonitrile exists in a β -turn type-I conformation having pro- and L-ala in I + 1 and I + 2 positions, respectively. The binding of calcium ion slightly distorts the structure with change a in the orientation of L-ala carbonyl facilitating the optimal binding of calcium ion. Possible lipid interaction was investigated using CD and DSC. CD studies showed that there was drastic change in the conformation of peptide on interacting with the lipid. DSC data also supported the CD results. The first neuropeptide taken for the study was acidic neurotransmitter NAAG present in the brain having important physiological functions. Detailed NMR studies in methanol showed that the peptide exists in a conformation having a γ -turn comprising the N-acetyl-asp group. Proton and ¹³C NMR studies on NAAG in water at different pH values indicated that the peptide exists as a dimer in well-defined conformations stabilized by a network of hydrogen bonds. CD and NMR studies on NAAG-polyamine complexes in methanol showed that NAAG binds to putrescine, cadaverine and spermine with high affinity. In the case of NAAG-putrescine complex, putrescine binds to α -COOH group and the side-chain COOH groups in NAAG without perturbing the γ -turn at the N-terminal region. In the case of NAAG-spermine complex, spermine binds to all the COOH groups leading to a completely extended conformation. The second class of neuropeptides taken for the study was arg-phe-amide peptides. Detailed structural studies were done on three different arg-phe-amide peptides. CD studies showed that phe-met-arg-phe-amide has higher binding affinity for calcium ion among the metal ions studied. NMR studies on seven-residue peptide, pgluc-asp-pro-phe-leu-arg-phe-amide in methanol, showed that it adopts an α -turn conformation having a γ -turn within, induced by Pro 3 residue. Detailed NMR studies on ten-residue arg-phe-amide peptide pro-asp-val-asp-his-val-phe-leu-arg-phe-amide in TMP showed that it adopts an α -turn conformation comprising the first five residues and a turn structure at the C-terminal having the last three residues.

References

1. VOET, G. J. AND VOET, D. *Biochemistry*, second edition. Wiley, 1995, p. 141.
2. HRUBY, V. J. *et al.* *Peptides: Chemistry and biology, Proc. 12th Am. Peptide Symp.*, (J. A. Smith and J. E. Rivier. eds), ESCOM, p. 142.
3. KARLE, I. L., *et al.* *Peptides, structure and function* (Hruby, V. J. and Rich, D. H. eds), Pierce Chem. Co., 1983, p. 291.
4. KESSLER, H., *et al.* *Angew. Chem. Int. Ed. Engl.*, 1992, **31**, 326.

Thesis Abstract (M.Sc. Engng)

Numerical analysis of dusty hypersonic viscous gas flow using 2D Navier–Stokes equations by R. Padmapriya

Research supervisor: Prof. K. P. J. Reddy

Department: Aerospace Engineering

1. Introduction

Most of the interplanetary explorations are dominated by hypersonic flight corridors. The re-entry aerodynamics of vehicles flying at hypersonic Mach numbers is an important aspect of most space missions. More often, the composition of the atmosphere, which the vehicle has to encounter, consists not only of gas other than pure air but also dust particles of varying dimensions. Further, in the case of Martian entry probes using ablative material for protection against severe aerodynamic heating, which occurs at high flight velocities, the products of ablation particles are also present giving rise to complex flows.¹ Therefore, it calls for a study of flows that is more realistic in nature, viz. two-phase flows.

The aerodynamics of the dusty gas flows has been analyzed extensively both theoretically and experimentally. Most of the reported theoretical analyses are based on boundary-layer approximations, whereas the flow field is governed by full Navier–Stokes (N–S) equations. Apart from this, many of these analyses restrict to a particular region in the flow field such as the stagnation point. These analyses, in spite of approximations involved at various levels, have given very good physical insight into the subject. Nevertheless, owing to approximations made in these analyses, their results will have limited application. Often, it is very difficult to say whether the solutions through these analyses are unique or not, unless a less approximate analyses confirms it.² Moreover, for cases where flow separation or a shock–shock or shock–boundary layer interaction occurs, such an analysis cannot be made. Thus, the present work aims at a more accurate study of gas–particle flows at hypersonic Mach number by solving complete 2D N–S equations coupled with particle–phase equations numerically. The analysis yields complete laminar compressible flow field around the flat plate.

2. Numerical algorithm

In the present analysis, it is assumed that the gas is perfect with constant specific heat and the particles are solid spheres with uniform diameter. The gas viscosity is given by Sutherland's law. Also, the volume occupied by the particle is neglected and the exchange between the two phases is through the Stokes drag for momentum transfer and convection for heat transfer. The basic N–S equations governing dusty gas flow in the conservative form are

$$(\partial U/\partial t) + (\partial F/\partial x) + (\partial G/\partial y) = H$$

where U is the conserved variable, F and G are inviscid and viscous fluxes and H represents the interaction source term between particles and gas phase. The mass, momentum and energy conservation equations for both particle and gas phases have been solved using finite-volume upwind schemes which incorporate natural dissipation. The equations governing the gas phase are solved using Roe's flux difference splitting algorithm.³ On the other hand,

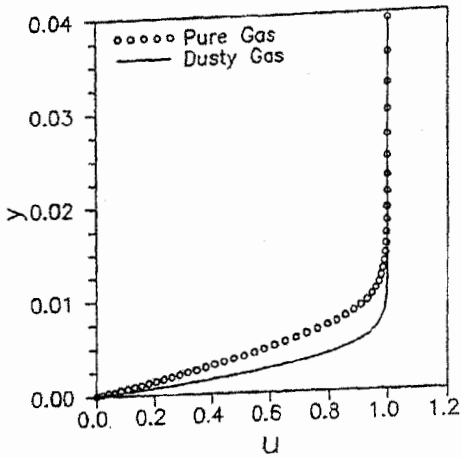


FIG. 1. Velocity profiles within the boundary layer over a flat plate at $x = 1.2$ for $M_\infty = 6$, $Re_\infty = 10^6$.

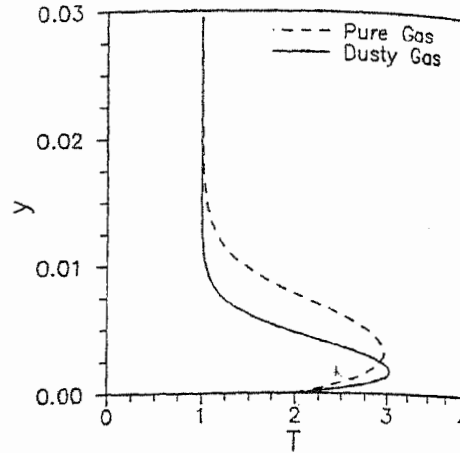


FIG. 2. Temperature profiles within the boundary layer over a flat plate at $x = 1.2$ for $M_\infty = 6$, $Re_\infty = 10^6$.

particle-phase equations are solved using Steger-Warming flux-vector-splitting technique.⁴ Totally eight equations, four each, for the gas and the particle phases have been solved with explicit coupling. The present method enables the capturing of shock profile accurately.

The problem is treated to two dimensions with 88×32 fine rectangular mesh. The upstream boundary conditions are the freestream conditions, where the gas and particle phases are in equilibrium. No slip conditions are assumed at the wall. The particles selected were uniform size glass spheres of $10 \mu\text{m}$ radius with constant material density. The numerical code is validated by regenerating the flow-field profiles reported in literature.⁵

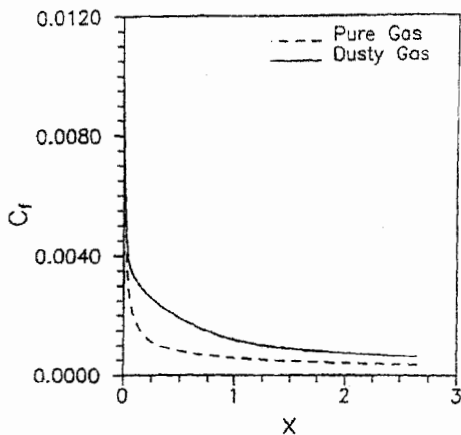


FIG. 3. Skin-friction variation along the flat plate for $M_\infty = 6$, $Re_\infty = 10^6$.

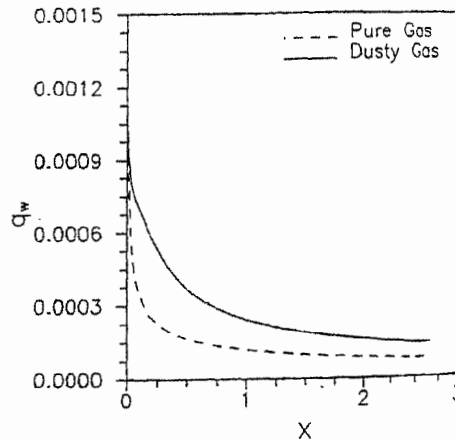


FIG. 4. Variation of wall heat transfer along the flat plate for $M_\infty = 6$, $Re_\infty = 10^6$.

3. Results

Typical velocity and temperature profiles generated for freestream Mach and Reynolds numbers of 6 and 10^6 , respectively, are shown in Figs 1 and 2. These figures indicate that the presence of the particles in the flow has an appreciable effect on the flow-field parameters. The variation of the skin friction coefficient and the heat-transfer rate along the length of the flat plate (Figs 3 and 4) shows that the presence of the particles in the flow enhances skin friction and wall heat transfer. This increase is due to the interaction between gas and particle phases leading to reduction of the boundary-layer thickness as evident from Figs 1 and 2. Complete details of the numerical techniques employed in the present analysis along with the results of the parametric and grid refinement studies will be reported in a full-length paper.

References

- 1 WALDMAN, G. D. AND REINECKE, W. G. *AIAA J.*, 1971, **9**, 1040–1048.
- 2 CHAMKHA, A. J. *J. Fluids Engng*, 1996, **118**, 179–185.
- 3 ROE, P. L. *J. Comp. Phys.*, 1981, **43**, 357–372.
- 4 STEGER, J. L. AND WARMING, R. F. *J. Comp. Phys.*, 1981, **40**, 263–293.
- 5 WANG, B. Y. AND GLASS, I. I. *J. Fluid Mech.*, 1988, **186**, 223–241.

Thesis Abstract (Ph. D.)

Single crystal structural investigation on the oligonucleotides $d(G_4CGC_4)$ and $d(C_4A_2C_4A_2)$ by G. Savitha

Research supervisor: Prof. M. A. Viswamitra

Department: Physics

1. Introduction

This work deals with structural investigations on usual and unusual forms of DNA. The first part deals with crystal structure solution of the A-DNA decamer $d(G_4CGC_4)$ at 1.9 Å resolution. This structure has many unique features to its credit in that the decamer crystallizes in the $P2_1$ space group with two independent molecules in the asymmetric unit which is an uncommon feature in A-DNA oligomers and seen for the first time. This arrangement has the advantage of studying the same molecule in different packing environments within the same crystal. The second part deals with crystallization and attempts at solving the structure of a C-rich telomeric repeat sequence $d(C_4A_2C_4A_2)$. It is the longest telomeric repeat studied crystallographically so far. It involved a lot of model building as there was no precedence to this structure when the present work was undertaken. Evidence from cross-rotation search points at an intercalated tetraplex structure with hemiprotonated C·C⁺ base pair. The intriguing nature of the structure was the major impetus in pursuing attempts at solving it, in spite of several experimental limitations.

2. Crystals of $d(G_4CGC_4)$

The molecular structure of the self-complementary decamer sequence $d(G_4CGC_4)$ was solved by X-ray diffraction analysis. The interest in this molecule comes from the fact that C/G-rich

sequences show a striking conformational versatility and has been the subject of interest of various groups, including our laboratory. It has been observed that interspersed stretches of G/C bases mostly favour the A form and alternating sequences favour the Z form. This oligonucleotide contains both types of sequences. The sequence d(G₄CGC₄) adopts an A-DNA conformation quite similar, on average, to that found in fibres.

The d(G₄CGC₄) sequence was one among the several GC-rich A-DNA decamers synthesized on an ABI-DNA synthesizer that could be crystallized. Crystals of d(G₄CGC₄) were grown by vapour diffusion method by adding sequentially 10 μ l drops of 2 mM DNA, 20 mM sodium cacodylate buffer (pH 6.5), MgCl₂, 2mM spermine tetrachloride and 5% MPD. It was equilibrated against a reservoir solution of 50% MPD. They belong to the monoclinic system with unit cell dimensions, $a = 45.504 \text{ \AA}$, $b = 46.084 \text{ \AA}$, $c = 28.465 \text{ \AA}$ and $\beta = 100.738^\circ$ in the space group P2₁ with two duplexes in the asymmetric unit ($\approx 12 \text{ kDa}$). Data collection and processing were made on the Imaging Plate System at the Molecular Biophysics Unit (MBU), Indian Institute of Science (IISc). The processed and reduced intensity data has an acceptable completeness and R-merge to 1.9 \AA resolution.

The solution of this structure was challenging as it had crystallized in an unusual space group, P2₁, for DNA oligomers, with more than one duplex in the asymmetric unit. The initial phasing was done by the molecular replacement method by first exploring homologous sequences of both A and B forms of DNA from the Nucleic Acid Data Bank as there are no isomorphous structures reported. The structure of d(CCGGC)r(G)d(CCGG)¹ proved to be an excellent model with the R-factor dropping to 39.6% and a correlation factor of 58.5% after one round of rigid body refinement. The decamer duplex adopts an A-DNA conformation. The two molecules in the asymmetric unit were found to be related by 182.24° along with a translational component and they were refined independently. Examination of electron-density maps and water fitting followed by position and b-group refinement yielded a final R-factor of 17.4% for 808 DNA atoms and 115 water molecules.

The two molecules in the asymmetric unit are related by near dyad symmetry in the ac-plane by groove interaction, with the end base pair of one molecule abutting into the minor groove of the other by making hydrogen bond contacts with three consecutive residues of the opposite strand. The minor groove is mostly involved in intermolecular contacts while the major groove is confined to the solvent and is the site of systematic hydration. The abrupt distortion of the backbone torsions α and γ , due to intermolecular contacts, shifts them to *trans* conformation from their favoured *gauche*⁻ and *gauche*⁺ conformations, respectively. In this close encounter, one of the molecules in the asymmetric unit suffers more deformations when compared to the other.

Molecule 1 has interactions which are distributed symmetrically unlike Molecule 2. As a result, Molecule 2 has larger deviations in terms of backbone torsions and helical parameters, especially C37 which shows a remarkable deviation in torsions α and γ , and a large roll in the centre of the helix.

An interesting aspect of this structure is that in spite of the intrinsic molecular symmetry of the d(G₄CGC₄) decamer, equivalent base pairs show significant differences in the two molecules in the asymmetric unit. The lack of symmetry should originate from intrinsic fea-

tures in the $d(G_4CGC_4)$ base composition, predisposing the structure to such intermolecular interactions which give optimal packing in the crystal or counterion binding. In summary, the situation found in the crystals indicates that the sequence, the oligomer length and crystallization solvent may all have a strong influence on the DNA form and structure adopted by oligonucleotides upon crystallization.

3. Crystals of $d(C_4A_2C_4A_2)$

Repetitive cytosine-rich DNA sequences have been identified in telomeres and centromeres of eukaryotic chromosomes. These sequences are crucial in structural stability of the chromosome besides its connection with cancer and aging. This unexplored area of repeat units based on natural sequences was chosen as the subject of study.

At the onset of this work, there were no DNA crystal structures reported with C-rich sequences consisting of self-paired DNA stabilised by pure base-stacking interaction and a parallel-stranded duplex. Several C-rich sequences which were mostly 12-mers (about 4kDa) were synthesised on the automated ABI-DNA synthesizer and several of them could be crystallized.

Extensive work was done on the *Tetrahymena* telomeric repeat sequence $d(C_4A_2C_4A_2)$. The crystals belong to the space group $P6_{4(2)}22$ with cell dimensions $a = 27.346 \text{ \AA}$, $b = 27.346 \text{ \AA}$ and $c = 184.458 \text{ \AA}$ with 12 nucleotides in the asymmetric unit. Though the crystals grew easily, much time had to be spent in growing crystals large enough for X-ray data collection. The crystals posed a lot to experimental problems as one of the axes is unusually long and the added susceptibility of the crystals to radiation damage in the X-ray beam within two to three hours of exposure made data collection a long-drawn process. Data were collected at the Area Detector Facilities at MBU, and Bath University. Finally, a 3.0 \AA -resolution data could be obtained with good data statistics.

The Patterson maps and self-rotation functions showed that the molecule was located at $(0, 0, z)$ in the crystal, so the structure solution involved finding the position and orientation of the molecule about c -axis and this seemed feasible by model building and using the molecular replacement method for structure determination. As there were no related crystal structures reported, structure solution involved *ab-initio* model building with inputs from small-molecule crystallography, fibre-diffraction data and solution studies which suggested at that time hemiprotonated cytosines which self-pair between two parallel strands to form duplexes. The duplex models with varied initial monomer parameters and helical parameters failed to give any solution. However, when an intercalated model as proposed by Gehring *et al.*² from NMR studies was used, the cross-rotation function searches proved promising. It also explains the 6.4 \AA spaced vectors in the Patterson maps. From the evidence of cross-rotation searches which is based on the philosophy of superposition and maximal overlap, when there is strong similarity between the model and the real structure, we are tempted to believe that $d(C_4A_2C_4A_2)$ is indeed a four-stranded structure.

The limiting 3 \AA data, the asymmetric cell which leads to the unstable packing of helices as continuous rods, the susceptibility of the crystals to X-rays and the multitude of possibilities

for the disposition of adenines in $d(C_4A_2C_4A_2)$ resulted in a serious handicap to solve the structure completely. Other crystallographic techniques like the isomorphous replacement method, using brominated derivatives and anomalous dispersion, also do not sound promising due to the latter reason, unless crystals with a reasonably symmetric cell that are stable in the X-ray beam can be obtained. Within these constraints, the maximum information that could be obtained has been harnessed and the structure of $d(C_4A_2C_4A_2)$ indeed comes within the family of i-motif structures.

References

1. BAN, C., RAMAKRISHNAN, B. AND SUNDARALINGAM, M. J. *J. Mol. Biol.*, 1994, **236**, 275–285.
2. GEHRING, K., LEROY, J. L. AND GUERON, M. *Nature*, 1993, **363**, 561–565.

Thesis Abstract (Ph. D.)

Characterizations and algorithms for subclasses of planar perfect graphs by S. Rengarajan

Research supervisor: Prof. C. E. Veni Madhavan
Department: Computer Science and Automation

1. Introduction

This work presents efficient algorithms for solving certain combinatorial problems on subclasses of planar-perfect graphs. The classes dealt with are planar chordal and planar permutation graphs. We study the underlying combinatorial of graph-theoretic structure and develop efficient algorithms based on these. A reason for studying classes such as planar chordal graphs is that planarity imposes nice structural requirements on the graph G and thus greatly facilitate design of fast algorithms on G . Another reason is the availability of good decomposability properties of chordal graphs.

We present new results on a practical linear time algorithm for deciding whether or not a planar chordal graph has a *Hamiltonian cycle*, thus settling the complexity status of Hamiltonicity problem for planar chordal graphs. We then address the problem of *book thickness* also known as *page number* for the class of 2-trees and extend a known result on maximal outer-planar graphs.¹ A constructive proof is presented to show that the page number (or *stack number*) of 2-trees is two. A related graph invariant called *queue number* of a graph was introduced by Heath and Rosenberg.² We extend known results to maximal outer-planar graphs (mops) and 2-trees by constructing two- and three-queue layouts, respectively. Next we show that the class of planar permutation graphs admit an elegant structural decomposition and using this we develop a simple linear time algorithm for recognizing a planar permutation graph in linear time. Also, using this structural decomposition result, we develop a linear time approximation algorithm for solving the *bandwidth minimization* problem on this class of graphs. Finally, we study *center graphs* of k -trees and give an efficient algorithm for finding centers. We give an outline of these results in the following sections.

2. Hamiltonian planar chordal graphs

A Hamiltonian cycle (path) of a graph G is a simple cycle (path) spanning all the vertices of G . The Hamiltonian cycle (HA) problem is that of determining whether a given graph contains a Hamiltonian cycle. The HA problem for general graphs is a well-known NP-complete problem.³ However, for certain restricted classes of graphs polynomial time algorithms have been developed to solve the problem. The problem remains NP-complete even if we restrict our attention to planar or chordal graphs.

Arnborg and Proskurowski⁴ present a general linear time algorithm for the Hamiltonian cycle problem for *partial k -trees*. The authors assume a sophisticated tree decomposition of partial k -trees and the algorithm is of the order of *double exponential* time in the *tree width* (fixed) k . In this work, we study the Hamiltonian cycle problem for planar chordal graphs, a subclass of partial-3-trees and give a simple and practical algorithm (i.e. one which does not involve huge constants).

We identify a subgraph structure called K_4^3 which is crucial in deciding whether G is Hamiltonian or not. We order the vertices of a planar-3-tree depending on how deep they are embedded in the inner faces with respect to the outer face and classify the vertices of a K_4^3 depending on their *level number*. By observing the nature of the Hamiltonian path P in a K_4^3 we fix the *end vertices* of P . Thus, we show how K_4^3 's can interact with one another at the end vertices. Based on the K_4^3 structure we stratify the faces of the planar-3-tree into *parent* and *children faces*. We generalize the notion of a K_4^3 into a *locally Hamiltonian $K_4(lh - K_4)$* and a *general K_4^3* . The Hamiltonian path is extended from inner-most K_4^3 to its parent face following two traversal rules. We define a notion of *blocking* vertices to identify the vertices which terminate the recursive process of augmenting a Hamiltonian cycle. Then we show:⁵

Theorem 1: *A planar-3-tree G is Hamiltonian if and only if for each general K_4^3 A of G all three external vertices of A are not blocking vertices. The proof of the theorem gives a simple linear time algorithm to detect planar Hamiltonian graphs.*

Another important feature of the work is that we present a constructive definition for generating planar chordal graphs from planar-3-trees. This is of independent interest. Using this definition we extend the above result to planar chordal graphs. We extend the concept of blocking vertex to a *blocking edge* or a *blocking triangle*. We characterize the Hamiltonian planar chordal graphs by the following theorem.

Theorem 2: *A planar chordal graph G is Hamiltonian if and only if*

- *G does not have a blocking vertex, blocking edge, and a blocking triangle.*
- *for each general K_4^3 , A , of G all three external vertices of A are not blocking vertices.*

We use this theorem to develop a linear time algorithm for testing hamiltonicity of planar chordal graphs.⁶

3. Stack and queue number of 2-trees

A *book embedding* of a graph consists of an embedding of its vertices along the spine of a book (i.e. a linear ordering of the vertices) and an embedding of its edges on the pages so that the edges embedded on the same page do not intersect. The minimum number of pages required to book embed a graph is called the *page number* or *book thickness* of the graph. The book-embedding problem for a graph is to determine the page number and to give an embedding using the minimum number of pages. The page number of a graph is also called the *stack number* of a graph. It is NP-complete to decide whether a given graph has a two-page book embedding. However, for special classes of graphs such a book embedding can be found in polynomial time. Trees and outer planar graphs have been shown to have one-page book embedding. We extend this result and *show* that 2-trees require two pages for book embedding. Analogous to the stack number of a graph another graph invariant is the *queue number* of a graph. Graphs requiring exactly 1-queue are characterized by Heath and Rosenberg.² It is NP-complete to decide whether or not a given graph admits a 1-queue layout. We show that maximal outer planar graphs require 2- and 3-queues are sufficient for 2-trees. We modify the proof of the 1-queue layout of leveled arched planar graphs³ to show that mops require 2-queues and we exhibit a 2-queue layout for mops. As this proof technique cannot be extended to 2-trees we define a notion of 2-chain and show that the class of 2-trees has a 3-queue layout.⁶

4. Planar permutation graphs and bandwidth minimization

Planar permutation graphs (ppg) play an important role in wire layout and other problems. Fast recognition of planar permutation graphs is an important problem. Though planar graphs can be recognized in linear time, checking whether the graph is a permutation graph takes $O(n^2)$ time. We present a linear time algorithm for recognizing whether a graph is a ppg. Our algorithm is a much simpler and faster alternative to the existing algorithm based on transitive orientation of associated comparability graphs. Our characterization of planar permutation graphs is entirely different from the known notions of permutation graphs. The *planarity* condition makes the permutation graphs 3-connected. Using planarity and 3-connectivity, we arrive at simple necessary and sufficient conditions for a graph to be a planar permutation graph. Using these conditions we develop a linear time algorithm to recognize planar permutation graphs.

Bandwidth minimization of a graph is a well-known combinatorial problem having many applications. However, this problem is NP-complete even for the class of trees. For *caterpillars* of hair length one graphs (a smaller class than trees) there exists a polynomial time algorithm for getting an optimal bandwidth. This class of graphs—caterpillars of hair length one—is a proper subclass of planar permutation graphs. We use our result on structural decomposition of planar permutation graphs to get an approximation algorithm for bandwidth minimization problem with a performance guarantee of 2.

5. Computing centers of k -trees

The centre of a graph is the set of vertices with minimum *eccentricity*. Eccentricity of a vertex v in G is the maximum of the shortest distance of v to each vertex in G . The center graph of

G is the vertex-induced subgraph of vertices which are centres of G . The centre graphs of trees are well known. Proskurowski⁷ extends the result to mops and 2-trees. We extend the above result to planar-3-trees. We also modify a structural result of Das and Rao⁸ on the diameter of center graphs of chordal graphs to compute the centers of k -trees efficiently.

References

1. CHUNG, E., LEIGHTON, T. AND ROSENBERG, A. L. Embedding graphs in books: A layout problem with applications to VLSI design, *SIAM J. Algebraic Discrete Meth.*, 1987, **8**, 33–58.
2. HEATH, L. S. AND ROSENBERG, A. Laying out graphs using queues, *SIAM J. Computing*, 1992, **21**, 927–958.
3. GAREY, M. R. AND JOHNSON, D. S. *Computers and intractability*, W. H. Freeman, 1979.
4. ARNBORG, S. AND PROSKUROWSKI, A. Linear time algorithms for NP-complete problems restricted to partial k -trees, *Discrete Appl. Math.*, 1989, **23**, 11–24.
5. RENGARAJAN, S. AND VENI MADHAVAN, C. E. Hamiltonian cycles in planar-3-trees, *National Seminar on Theoretical Computer Science-3*, IIT, Kharagpur, 1993, pp. 53–66.
6. RENGARAJAN, S. AND VENI MADHAVAN, C. E. Stack and queue number of 2-trees, *First Annual Computing and Combinatorics Conf.*, Xi'an, China, August 24–26, 1995.
7. PROSKUROWSKI, A. Centers of maximal outer planar graphs, *J. Graph Theory*, 1980, **4**, 75–79.
8. DAS, P. AND RAO, S. B. Centre graphs of chordal graphs, *Proc. Seminar on Combinatorics and Applications conducted in honor of Prof. S. S. Shrikhande on his 65th Birthday*, Indian Statistical Institute, Calcutta, December 14–17, 1982, pp. 81–94.

Thesis Abstract (Ph. D.)

Caching strategies and design issues in CD-ROM based multimedia storage by Vijnan Shastri

Research supervisors: Profs V. Rajaraman and H. S. Jamadagni

Department: Computer Science and Automation

1. Introduction

CD-ROMs have proliferated as a distribution media for desktop machines for a large variety of multimedia applications (targeted for a single-user environment) like encyclopedias, magazines and games. With DVD-ROM capacities (digital versatile discs—successors to CD-ROM) ranging from 4.7–10 GB being available in the near future and transfer speeds showing rapid improvement, they will, in addition to spawning new applications in the PC-desktop market, become an important component of low-cost video-on-demand (VoD) servers to store full-length movies and read-only-multimedia. In this work, we look at performance issues in multimedia storage in these two environments: the single-user desktop environment and the VoD environment.

2. CD-ROM in a single-user PC environment

CD-ROM-based content in desktop systems is highly interactive and consists of video, text and graphics. Due to its highly interactive nature, there are two major areas of concern which are related to the design and performance of the CD-ROM subsystem (which includes the drive, the interface and the software driver) and the application software:

- First is the ability of the drive to deliver multimedia streams at the real-time bandwidth demanded by applications and maintain continuity of these multimedia streams. Failure to do so results in reduced video quality due to dropped video frames by the player.
- Second is the inordinate delay suffered by the user¹ when she/he clicks on the video icon to see a video clip pertaining to the text which she/he is reading or when she/he turns a page on screen. We will refer to this delay as 'waiting time'.

In an effort to ensure the first point mentioned above and to try to solve the second problem, the designers of CD-ROM subsystems, for their part, are continuously trying to enhance performance by improving the retrieval rate (of the optical head), seek times and the I/O bus interface circuitry (which affects the transfer rate from the drive to system memory over the I/O bus).^{2,3} Specifically, the retrieval rate and bus transfer rate affect the playback of continuous multimedia streams and seek time affects the 'waiting time'. However, while doing so, they are faced with several design trade-off issues such as:^{4,5}

- What is the optimal size of the onboard prefetch FIFO buffer (which is used to buffer data retrieved by the CD head but not yet transferred to system memory)?
- Can a main-memory-hosted cache improve performance and if so, how should it be designed and what are its design parameters?
- Is there a need for the cache to be adaptive in terms of its line size and total size and if so, how should this be implemented?
- Should design effort be directed to improve long throw seek time (involving movement over a large radial distance) or short throw seek time (involving movement to a neighboring track)?

Our goal is to seek answers to these questions and to see if caching can help alleviate the 'waiting time' problem. These issues can be correctly addressed only if they are studied in the context of the actual applications being run. Hence, we take a very pragmatic approach in which we make a detailed study of application behaviour in terms of I/O request patterns generated to the CD-ROM subsystem by tracing these patterns. We then take the trace-driven-simulation approach for analysis. We have put in a lot of effort to write a background program which intercepts the CD-ROM device driver, copies information from the I/O request packet and logs the traces into a file transparently to the user.

3. DVD-ROMs in VoD environment

DVD-ROMs of 4.7–10 GB capacities are expected shortly. This will mean that a single movie of 133-minute duration can be stored at MPEG-2 data rate (average rate is 5Mbits/s) on

a single DVD-ROM and at a very low cost per byte. The cost of the video server (in addition to the costs of the network) is a major issue in the deployment of video-on-demand systems. The increasing transfer speed of CD-ROM drives (and a similar expected trend in DVD-ROM drives) implies that more than one request (video stream) can be served by a single drive and they can be used directly as components of video pumps (dedicated video storage). These DVD-ROM video pumps are the building blocks for video servers in a VoD environment and not just the next-level storage (to magnetic RAID servers) in a memory hierarchy system. DVD-ROMs will be specifically used in read-only VoD applications such as movie-servers.⁶

CD-ROM towers and magnetic RAID towers will be used as ‘video pumps’.⁷ This implies that the operating system and index data for the movies will not reside on the video pumps. Hence the requests to the video pump will be purely for multimedia data and will be periodic. Multimedia request streams have a continuity rather than a latency requirement while the opposite is true for non-multimedia requests in traditional systems. This is the basis for our analysis of disk scheduling and buffer design and where we differ from previous research in this area which has optimized performance for systems where both types (periodic multimedia requests and aperiodic requests) are present.

We first develop a computationally inexpensive algorithm to work out the service time per request knowing the seek-time overheads. We show that, in the light of the seek time characteristics that CD-ROM drives have, C-SCAN is twice as efficient (in terms of buffer requirements) as the popular SCAN algorithm. We then look at admission control and propose a ‘full-load’ admission control algorithm to admit new requests. We show that this algorithm not only supports VCR-like operations such as fast-forward, fast-rewind and pause but can handle VBR (variable bit rate) video streams such as MPEG-2 as well. Previous work in this area does not deal with the problem of disk scheduling for VBR streams, admission control, and handling of VCR-like requests in an integrated manner. We then do extensive simulation of our algorithm and use it to extract parameters such as disk bandwidth utilization factor, cycle time and additional buffer sizes needed. Our contribution is that our algorithm integrates all these functions in a video pump.⁸

4. Contribution of this work and conclusions

4.1. *In a single-user desktop environment*

- We have developed a trace program (running in the background transparently to the user) that intercepts the CD-ROM device driver and is able to collect and store traces (the I/Q request information from application to CD-ROM). We use these traces to do trace-driven simulation and analysis.
- In addition, we have written programs to obtain the seek time profile of the CD-ROM drive, raw transfer rate, bus-interface speed, and buffer size of the drive.
- Our traces show that at least 70% of all accesses are contiguous and the role of the prefetch buffer is crucial for this type of access. Prefetch buffer design is discussed and we derive a general relationship to calculate the prefetch buffer size on the CD-ROM

drive that takes into account the rotational delay and the continuity requirement of multimedia streams. We then show that it is better to place multimedia data near the centre of the disc. We show through measurement that contiguous sector reads do not incur a seek overhead and deduce that a main memory cache cannot play any role for contiguous sector access.

- We present the design parameters of a main memory-hosted cache that looks at non-contiguous requests. We work out the cache line size and the cache size based on simulations from our traces. Our analysis shows that the line size should be chosen such that fetching a line does not incur overhead of more than 20% of the 100-sector seek distance for that drive. For a fixed sized cache, we find that a 1MB cache gives results almost as good as a cache of unlimited size. Since we find that the performance of the cache varies within and across sessions, we present a scheme by which the cache monitors its own performance and adapts its size based on the seek characteristics and data transfer speed of the drive. We show that size-adaptation results in a three-fold saving in terms of memory occupied by the cache.
- We show (from our traces) that short seek distances are important, not the often quoted full-stroke or 1/3rd stroke seek times. Our seek-time measurements show that when the CD-head seeks to a new position on the CD, the head-seeking time dominates over the time to change the rotational speed of the drive.

4.2. *In the video-on-demand environment*

- We present a quantitative relationship to calculate the service time for each request given the playback rates and seek-time overheads.
- Using our seek-time measurements of the CD-ROM drive we prove that the C-SCAN algorithm is optimal for CD-ROM drives.
- We then present a 'full load' admission control algorithm that guarantees continuity of playback for all requests even when requests are admitted or deleted for variable bit-stream (VBR) multimedia streams.
- We discuss the implementation of this admission control algorithm where we show that it can handle operations such as fast-forward, rewind and pause using an index table for the CD-ROM drive.
- We then simulate the algorithm and run it against VBR streams and extract parameters such as cycle time, disk bandwidth utilization factor and additional buffer sizes needed to meet sporadic demands for bandwidths that exceed that of the disk.

References

1. GEMMEL, D. J. *et al.* Delay sensitive multimedia on disks, *IEEE Multimedia*, Fall 1994, 56–66.
2. RUEMMLER, C. AND WILKES, J. An introduction to disk drive modelling, *IEEE Computer*, 1994, 27, 17–30.

3. SMITH, A. J. Disk cache-miss ratio analysis and design considerations, *ACM Trans. Computer Systems*, 1985, **3**, 161–203.
4. PATTERSON, D. AND HENNESSEY, J. *A quantitative approach to computer architecture*, Morgan Kaufmann, 1990.
5. GEMMEL, D. J. *et al.* Multimedia storage servers—a tutorial, *IEEE Computer*, 1995, **28**, 40–49.
6. RANGAN, P. V. AND VIN, H. M. Designing file systems for digital video and audio, *Operating Systems Rev.*, 1991, **25**, 69–79.
7. CHANG, E. AND ZAKHOR, A. Cost analysis for VBR video servers, *IS&T/SPIE Conf. on Multimedia Computing and Networking* 1996, pp. 381–397.
8. SHASTRI, V., *et al.* Performance issues in CD-ROM based storage systems for multimedia, *IEEE Conf. on Multimedia Computing and Systems*, Hiroshima, Japan, June 1996, pp. 151–155.

Thesis Abstract (Ph. D.)

Modelling and analysis of voltage source converter based FACTS controllers for real and reactive power control by A. M. Kulkarni

Research supervisor: Prof. K. R. Padiyar

Department: Electrical Engineering

1. Introduction

The concept of flexible AC transmission systems (FACTS) envisages the use of high-power electronic controllers to improve system operation by fast and reliable control.

The first generation of FACTS devices like SVCs have been operated successfully and prototype installations of TCSC have shown promising results.

The new generation of FACTS controllers which are being developed are based on voltage source converters (VSC) which use self-commutating devices like GTOs. These controllers require lower ratings of passive elements (inductors and capacitors) and the voltage source characteristics present several advantages over conventional variable impedance controllers. The three basic VSC-based controllers are static condenser (STATCON, used for shunt compensation), static synchronous series compensator (SSSC used for controllable series compensation) and unified power flow controller (UPFC, both shunt and series compensation).

The basic concept of using VSCs for dynamic compensation of AC transmission lines was discussed by Gyugyi.¹ Subsequent papers by Gyugyi *et al.*^{2,3} describe the UPFC and SSSC in detail. A large prototype (+100 Mvar) of STATCON has already been installed.⁴

The application of FACTS controllers brings up new challenges for power engineers, not only in hardware implementation, but also in design of control systems, planning and analysis. In particular, the effective utilisation of these controllers will depend on the development of optimal control strategies. Due to the fast response of such controllers, one has to deal with

a wide spectrum of transient behaviour, including network dynamics, generator rotor (low frequency) oscillations and torsional oscillations.

The work can be classified into two parts

- (i) Modelling, analysis and control of STATCON, SSSC and UPFC using detailed models with emphasis on network (fast) dynamics and primary control strategies.
- (ii) Modelling and study of (auxiliary) control strategies to damp low-frequency power swings using linearised and simplified models.

2. Modelling and analysis of STATCON

The basic equations (ignoring harmonics) are formulated in the D–Q reference frame. The results obtained from analysis of these equations and detailed digital simulation are correlated.

An investigation is carried out on the use of fuzzy controller for reactive current control, in the light of the fact that the system is not amenable to linear feedback control. With this controller, the problem of small-signal instability in inductive region is mitigated and the nature of response is insensitive to operating point variations. Also, the controller is robust to change in plant brought about by the introduction of detailed network dynamics.

The nature of plant-transfer function for voltage regulation at the midpoint of a long transmission line using reactive current control is investigated.

An important observation is that the plant-transfer function for voltage regulation generally has a zero on the positive real axis of the complex plane. This precludes the use of high gains if an integral or PI controller is used as it tends to destabilize an oscillatory mode.

A compensator in cascade with an integral controller is designed to overcome this problem.

There is excellent correlation between the results obtained from simplified analysis, linearized eigen analysis of detailed model and digital simulation. While the system is admittedly very complex, it is shown that some analytical development is possible and is very fruitful in diagnosing and understanding control problems.

3. Development of control strategy for UPFC

A control strategy is proposed for UPFC wherein real power flow through the line is controlled, while regulating magnitudes of the voltages at its two ports. A controller is designed for this purpose which uses only local measurements. The control strategy is evaluated using transient digital simulation for a case study.

The salient features of the control strategy are:

- (i) Real power flow control by reactive voltage injection.
- (ii) Indirect reactive power flow control by control of voltage at the two ports of UPFC.

The simulation results for a case study indicate that this is a viable control scheme.

It is shown that by modulating the active power it is possible to bring about a vast improvement in transient stability and damping.

4. Sub-synchronous resonance study with SSSC-compensated transmission line

The problem of sub-synchronous resonance (SSR) is a major concern in the series compensation of a transmission line. SSR studies on a system (IEEE first benchmark system) with series compensation provided by SSSC are carried out. Eigenvalue analysis and digital simulation are performed to show that while constant reactive voltage injection by SSSC does not contribute to SSR, the problem may be present if it is used in combination with fixed compensation. A simplified analysis (damping and synchronising torque analysis) is carried out to suggest a control strategy to damp all modes including the electromechanical swing mode.

Simulation results presented bring out the effectiveness of this strategy.

5. Development of models of FACTS controllers suitable for small-signal analysis of low-frequency oscillations associated with generator rotor swing

The issue of modelling of FACTS controllers suitable for small-signal stability studies of low-frequency oscillations associated with generator rotor swings is also addressed. The following two issues in the incorporation of FACTS device dynamics into small-signal stability programs are discussed:

- (i) Development of suitable linearized models for FACTS devices.
- (ii) Interfacing the dynamical equations of FACTS controllers with the other system component models.

Incorporation of these models into small-signal stability programs is done systematically by representing the devices as dynamical subsystems connected to static network represented by admittance matrix. Series elements are represented as dynamical voltage injection; shunt-connected devices are represented as dynamical current injections into the network. For the sake of completeness, modelling of SVC and TCSC is also included.

Case studies are presented for a three-machine system with STATCON, SVC, TCSC, SSSC and UPFC.

6. Identification of control signals, control laws and optimal location of FACTS controllers in a unified framework to damp low-frequency oscillations

The work reported is aimed at identification of control signals, control laws and location of FACTS controllers in a unified framework, to damp the swing (electromechanical) modes.

A network analogy of the electromechanical system is used to suggest control laws. The signals required to achieve optimal damping for a given location are locally available. They can be obtained from the voltage across the FACTS device and the current flow through it.

The method is validated using detailed models of 3- and 10-machine systems. The study is carried out both for series and shunt compensations.

References

1. GYUGYI, L. Dynamical compensation of AC transmission lines by solid state synchronous voltage sources, *Trans. IEEE*, 1994, **PWRD-9**, 904-911.
2. GYUGYI, L. Static synchronous series compensator: A solid state approach to the series compensation of transmission lines, *Trans. IEEE*, 1997, **PWRD-12**, 406-417.
3. GYUGYI, L. The unified power flow controller: A new approach to power transmission control, *Trans. IEEE*, 1995, **PWRD-10**, 1085-1099.
4. SCHAUDER, C. *et al.* Development of +100 Mvar static condenser for voltage control of transmission systems, *Trans. IEEE*, 1995, **PWRD-10**, 1486-1496.